



Precise breakpoint detection in a patient with 9p– syndrome

Jeffrey Ng,¹ Eleanor Sams,¹ Dustin Baldrige,² Milinn Kremitzki,³ Daniel J. Wegner,² Tina Lindsay,³ Robert Fulton,³ F. Sessions Cole,² and Tychele N. Turner¹

¹Department of Genetics, Washington University School of Medicine, St. Louis, Missouri 63110, USA; ²Edward Mallinckrodt Department of Pediatrics, Washington University School of Medicine, and St. Louis Children's Hospital, St. Louis, Missouri 63110, USA; ³McDonnell Genome Institute, Washington University School of Medicine, St. Louis, Missouri 63110, USA

Abstract We present a case of 9p– syndrome with a complex chromosomal event originally characterized by the classical karyotype approach as 46,XX,der(9)t(9;13)(p23;q13). We used advanced technologies (Bionano Genomics genome imaging and 10× Genomics sequencing) to characterize the location of the translocation and accompanying deletion on Chromosome 9 and duplication on Chromosome 13 with single-nucleotide breakpoint resolution. The translocation breakpoint was at Chr 9:190938 and Chr 13:50850492, the deletion at Chr 9:1–190938, and the duplication at Chr 13:50850492–114364328. We identified genes in the deletion and duplication regions that are known to be associated with this patient's phenotype (e.g., *ZIC2* in dysmorphic facial features, *FOXD4* in developmental delay, *RNASEH2B* in developmental delay, and *PCDH9* in autism). Our results indicate that clinical genomic assessment of individuals with complex karyotypes can be refined to a single-base-pair resolution when utilizing Bionano and 10× Genomics sequencing. With the 10× Genomics data, we were also able to characterize other variation (e.g., loss of function) throughout the remainder of the patient's genome. Overall, the Bionano and 10× technologies complemented each other and provided important insight into our patient with 9p– syndrome. Altogether, these results indicate that newer technologies can identify precise genomic variants associated with unique patient phenotypes that permit discovery of novel genotype–phenotype correlations and therapeutic strategies.

Corresponding author:
tychele@wustl.edu

© 2020 Ng et al. This article is distributed under the terms of the Creative Commons Attribution-NonCommercial License, which permits reuse and redistribution, except for commercial purposes, provided that the original author and source are credited.

Ontology terms: autism; butterfly vertebrae; congenital sensorineural hearing impairment; hemivertebrae; profound global developmental delay; superior mesenteric artery aneurysm

Published by Cold Spring Harbor Laboratory Press

doi:10.1101/mcs.a005348

[Supplemental material is available for this article.]

INTRODUCTION

9p– syndrome, also referred to as Alfi's syndrome, is a genetic condition resulting from deletions on the p arm of Chromosome 9 (Alfi et al. 1973, 1976). However, the specific locations of these deletions can vary among affected individuals. No consensus about a critical region for this syndrome has emerged (Christ et al. 1999; Kawara et al. 2006; Hauge et al. 2008; Swinkels et al. 2008; Mitsui et al. 2013). In addition, genotype–phenotype correlation is confounded by unbalanced translocation events in about half the cases (Huret et al. 1988). Although the phenotypic characteristics of developmental delay and characteristic facies are common, other phenotypic characteristics (e.g., cardiac deficits) are more variably expressed (Huret et al. 1988; Swinkels et al. 2008).

Available genomic technologies permit detection of complex genomic variants with single-nucleotide breakpoint resolution (Eichler 2019). Using Bionano Genomics (Demaerel

et al. 2019) and 10× Genomics (Daiger et al. 2019) to characterize the cytogenetic events and genomic background of an individual with 9p– syndrome, we demonstrate characterization of genomic breakpoints with far greater resolution than array-based approaches (Bi et al. 2013) and identification of relevant genomic background variants. Specifically, these newer genomic technologies enable detection of the translocation event, determination of the exact base pair of the breakpoint, and decoding the sequence variation on the allele opposite of the deletion and throughout the rest of the genome. This case study provides insight into future clinical applications of these genomic technologies, into the utility of fine-resolution assessment of patient genomes, and into their putative application in genotype–phenotype correlations and discovery of novel therapeutic genomic targets.

RESULTS

Patient Phenotype Information

Our patient (9p.101.p1) is a 19-yr-old female with 9p– syndrome who had a clinical karyotype in 2001 of 46,XX,der(9)t(9;13)(p23;q13). She was born at 36 wk gestation with no other complications of pregnancy or delivery and no significant family history. At birth, dysmorphic facial features were noted with increased nuchal skin folds, left posterior polydactyly, and bicuspid aortic valve. Additional phenotypic features observed in the first 4 yr of life include global developmental delay, autism spectrum disorder, recurrent ear infections, bilateral sensorineural hearing loss, scoliosis (status post–spinal fusion at age 14 yr) associated with vertebral anomalies (hemivertebra at T10 and butterfly vertebrae at T5, T7, T8, and T11), and superior mesenteric artery syndrome, which has not required surgical intervention.

Genomic Analyses

Quality Check of 10× Genomics Data

Using the 10× Genomics platform, we achieved a coverage depth of $54.4 \pm 18.7\times$ with 98.2% of reads mapped and 86.5% of reads properly paired (see also Supplemental Table S1).

Precise Translocation Breakpoint Detection

Using the Bionano platform, we detected a translocation event between Chromosome 9 and Chromosome 13. With the BspQI enzyme map, the hg38 locations of the breakpoints were Chr 9:191412 and Chr 13:50852192, and with the BssSI enzyme map, the locations of the breakpoints were Chr 9:199014 and Chr 13:50853752 (Table 1; Fig. 1A). The 10× Genomics data revealed breakpoint locations of Chr 9:190929 and Chr 13:50850485 (Fig. 1B). Finally, read depth profiling of the 10× Genomics data followed by Integrated Genomics Viewer (IGV) (Robinson et al. 2011) inspection at the predicted breakpoint identified the exact breakpoints at Chr 9:190938 and Chr 13:50850492 (Fig. 2). These combined analyses revealed that Bionano and 10× Genomics technologies can identify the translocation event with resolution of ~400–8000 bp and 7–9 bp, respectively. Using a custom read depth calculation and IGV visualization approach, the 10× Genomics data ultimately permitted detection of the single-nucleotide breakpoints of this event.

Breakpoints of Accompanying Deletion and Duplication

Through our assessment of read depth from the 10× Genomics data, we also identified the deletion on Chromosome 9 and the duplication on Chromosome 13 that accompany the translocation event. The deletion location was Chr 9:1–190938 (Fig. 2A), and the duplication location was Chr 13:50850492–114364328 (Fig. 2B).

Table 1. Translocation event in 9p.101.p1

Technology	Chromosome	Breakpoint location (hg38)	Distance from actual breakpoint
Bionano BspQI map	9	191,412	474
Bionano BssSI map	9	199,014	8076
10×	9	190,929	-9
Actual breakpoint after read depth and IGV assessment	9	190,938	0
Bionano BspQI map	13	50,852,192	1700
Bionano BssSI map	13	50,853,752	3260
10×	13	50,850,485	-7
Actual breakpoint after read depth and IGV assessment	13	50,850,492	0

Other Related Genetic Events and Potential Phenotypic Consequences

By querying the existing literature, we identified genes in the large deleted and duplicated regions of our patient that are associated with phenotypic characteristics present in our patient (Table 2). We found seven genes associated with dysmorphic facial features, 11 genes with polydactyly, one gene with bicuspid aortic valve, 29 genes with developmental delay, 25 genes with autism, 20 genes with hearing loss, and six genes with scoliosis. We could not find genes associated with increased nuchal skin folds, left posterior polydactyly, coarctation

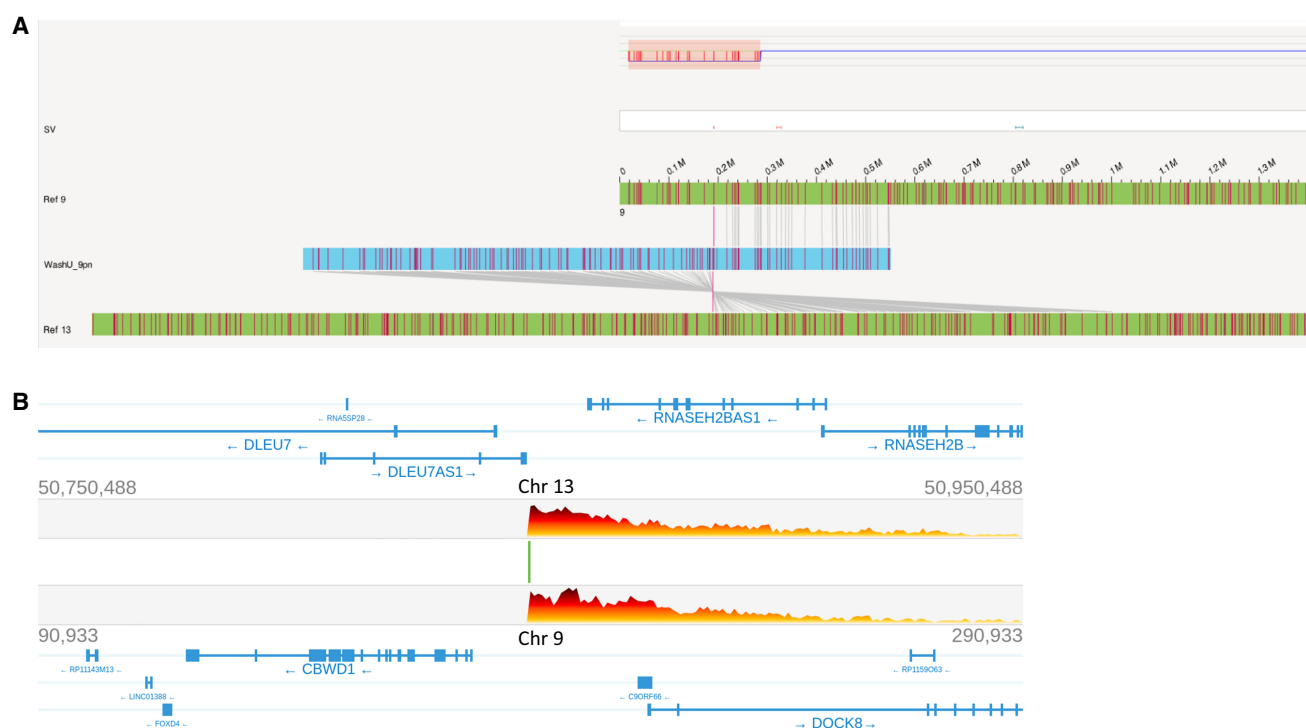


Figure 1. Variant detection by Bionano and 10× technologies. (A) BspQI map of the Bionano (hg19) data showing the location of the translocation breakpoint. (B) Loupe browser view (on hg38) of the translocation breakpoint in the 10× data.

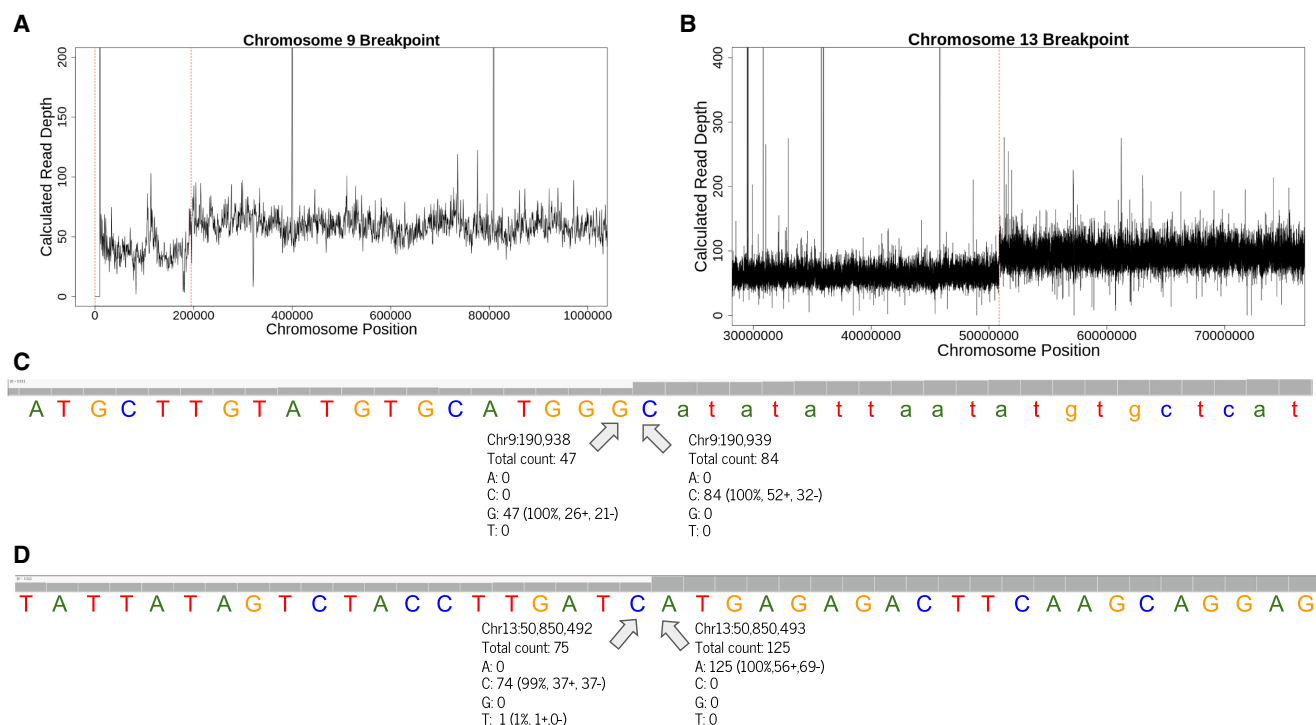


Figure 2. Precise breakpoint detection of the complex structural variant using the read information (on hg38). (A) Read depth profiling of Chromosome 9 exhibiting the deletion. (B) Read depth profiling of Chromosome 13 showing the duplication. (C) IGV view of the exact nucleotide of the translocation breakpoint on Chromosome 9. (D) IGV view of the exact nucleotide of the translocation breakpoint on Chromosome 13.

of the aorta, recurrent ear infections, ear infections, vertebral abnormalities, hemivertebrae, butterfly vertebrae, and superior mesenteric artery syndrome.

Loss-of-Function Variants in the Genome

We assessed single-nucleotide variant (SNV)/indel data for potential loss-of-function variants both within the deletion/duplication regions and also in the remainder of the genome. In particular, we focused on variants with an allele frequency of <1% in gnomAD (Karczewski et al. 2019). There were no variants matching these criteria within the deletion/duplication region. However, we did identify variants matching these criteria in the remainder of the genome, but these were in genes that did not have any known association with the patient's phenotype (Table 3).

DISCUSSION

Advancing genomic technologies are enabling precise resolution of complex structural variants. An example of a syndrome with these complex events is 9p- syndrome. In this syndrome, patients do not all share the same breakpoints, and approximately half of them also have translocations that involve Chromosome 9 and another chromosome. This complexity in event type is not limited to 9p- syndrome and confounds genotype-phenotype correlations. Classical strategies for characterizing patients with this syndrome include karyotyping to detect the deletion and possible translocation followed by an array-based

Table 2. Literature query for patient phenotype and genes within the deletion and duplication regions

Phenotype	Chromosome 9 deletion region (1–190938) genes	Chromosome 13 duplication region genes (50850492–114364328)		
Dysmorphic facial features		<i>CHAMP1</i> (1) <i>KLF12</i> (1) <i>MIR17HG</i> (1)	<i>ZIC5</i> (1) <i>ZIC2</i> (2) <i>GPC5</i> (1)	<i>LIG4</i> (6)
Polydactyly		<i>CKAP2</i> (1) <i>SUGT1</i> (1) <i>DIAPH3</i> (1) <i>RASA3</i> (1)	<i>GPC6</i> (1) <i>ZIC2</i> (2) <i>TFDP1</i> (1) <i>GRK1</i> (1)	<i>MIR17</i> (1) <i>GPC5</i> (2) <i>GAS6</i> (1)
Bicuspid aortic valve		<i>MIR17HG</i> (1)		
Development(al) delay	<i>FOXD4</i> (2)	<i>RNASEH2B</i> (3) <i>ATP7B</i> (3) <i>ALG11</i> (2) <i>PCDH8</i> (1) <i>PCDH17</i> (1) <i>CDC16</i> (1) <i>PCDH9</i> (1) <i>PIBF1</i> (1) <i>FBXL3</i> (1) <i>EDNRB</i> (2)	<i>NALCN</i> (10) <i>ADPRHL1</i> (1) <i>EFNB2</i> (2) <i>ARGLU1</i> (1) <i>LIG4</i> (11) <i>CHAMP1</i> (3) <i>COL4A1</i> (7) <i>COL4A2</i> (2) <i>ARHGEF7</i> (1)	<i>MIR17HG</i> (2) <i>GPC5</i> (2) <i>GPC6</i> (3) <i>TGDS</i> (1) <i>ZIC2</i> (6) <i>PCCA</i> (2) <i>DCUN1D2</i> (1) <i>TMCO3</i> (1) <i>TFDP1</i> (1)
Autism		<i>COL4A1</i> (3) <i>PCDH8</i> (3) <i>PCDH17</i> (3) <i>DIAPH3</i> (3) <i>PCDH20</i> (2) <i>PCDH9</i> (6) <i>IRS2</i> (3) <i>SPRY2</i> (1) <i>SLITRK1</i> (1)	<i>FARP1</i> (1) <i>ZIC2</i> (1) <i>NALCN</i> (2) <i>FGF14</i> (3) <i>METTL21C</i> (1) <i>DAOA</i> (2) <i>MYO16</i> (3) <i>MCF2L</i> (2)	<i>SLITRK5</i> (2) <i>MIR17HG</i> (1) <i>MIR17</i> (1) <i>GPC5</i> (2) <i>GPC6</i> (2) <i>KLF12</i> (1) <i>CARS2</i> (8) <i>UPF3A</i> (2)
Hearing loss		<i>ATP7B</i> (2) <i>ALG11</i> (1) <i>DIAPH3</i> (10) <i>PCDH20</i> (1) <i>DACH1</i> (1) <i>LMO7</i> (1) <i>ZIC5</i> (1)	<i>EDNRB</i> (30) <i>SPRY2</i> (4) <i>SLITRK6</i> (6) <i>IRS2</i> (2) <i>MIR17HG</i> (1) <i>DNAJC3</i> (1) <i>CDC16</i> (2)	<i>ZIC2</i> (3) <i>OXGR1</i> (1) <i>TMTC4</i> (1) <i>ERCC5</i> (2) <i>EFNB2</i> (1) <i>ARGLU1</i> (1)
Scoliosis		<i>RNASEH2B</i> (1) <i>ATP7B</i> (1)	<i>ZIC2</i> (1) <i>NALCN</i> (3)	<i>GRK1</i> (1) <i>ZIC5</i> (1)
Increased nuchal skin folds				
Left posterior polydactyly				
Coarctation of the aorta				
Recurrent ear infections				
Ear infections				
Vertebral abnormalities				
Hemivertebrae				
Butterfly vertebrae				
Superior mesenteric artery syndrome				

Numbers in parentheses indicate the number of supporting publications.

Table 3. Loss-of-function variants identified in 9p.101.p1 with an allele frequency < 1% in gnomAD

Chromosome	Position (b38)	Reference allele	Alternate allele	Consequence	Gene	HGVSc	HGVSp	gnomAD pLI	gnomAD o/e
8	19,361,315	G	A	Splice donor variant	<i>SH2D4A</i>	NM_001174159.1: c.706 + 1G > A	-	0	1.05
5	62,494,113	C	T	Stop gained	<i>IPO11</i>	NM_016338.4: c.1579C > T	NP_057422.3:p.Gln527Ter	0	0.28
7	102,285,252	G	T	Stop gained	<i>SH2B2</i>	XM_005276976.3: c.94G > T	XP_005277033.1: p.Glu32Ter	0	0.54

microarray for breakpoint resolution. However, these approaches limit identification of potential genotype–phenotype correlation and therapeutic targets because of genomic resolution (>50 kb).

We focused on one patient with 9p– syndrome who has been assessed in our genetics clinic. Classical karyotyping, 19 yr ago, revealed the translocation in this individual. However, the exact breakpoints of the translocation and associated deletion/duplication were unknown. With the advent of newer genomic technologies, we chose to test whether genome imaging with Bionano Genomics Saphyr system and/or 10× Genomics technologies could enable precise breakpoint detection. These two complementary methods were close to identifying the exact breakpoint and our manual assessment of these results enabled us to narrow down to the exact nucleotide position for each breakpoint. Future steps for this work would include the development of a read-based assembler near the putative breakpoints to automate the exact breakpoint detection. Of the two technologies, the 10× Genomics platform had the added benefit of inspection of sequence variants in the remainder of the genome.

Within the Chromosome 9 deletion and Chromosome 13 duplication regions we found genes that are associated with some of the phenotypes in our patient. This information was helpful for the assessment of our first patient. However, additional patients, sequenced at the same resolution, are required to make broad genotype–phenotype characterizations about 9p– syndrome. Because the list of potential genes involved in our patient’s phenotype is long, there are at least two future strategies for accurate and efficient genotype–phenotype characterization: (1) more precise patient phenotyping and (2) functional testing of genes in these regions. Outside of the deletion and duplication region we assessed loss-of-function variants because their functional consequence is predictable. Future areas of this work include assessment of missense and potential noncoding regulatory variants (e.g., in a promoter).

Application of newer genomic technologies allowed single-nucleotide resolution of the complex sequence variation in our patient with 9p– syndrome. This type of work is critical for the future of precision medicine and is the first step toward a better understanding of human phenotypes.

METHODS

Bionano Optical Mapping

We extracted high-molecular-weight (>50 kbp) DNA from the patient’s peripheral blood cells and subsequently labeled the DNA at specific sequence motifs using the Blood and Cell Culture DNA Isolation Kit and NLRS DNA Labeling Kit (Bionano Genomics 80004 and 80001) and nicking enzymes Nt.BspQI and Nb.BssSI (New England Biolabs R0644 and R0681, respectively) as described in respective protocols. The labeled genomic DNA

was linearized in nanochannel arrays in a Saphyr chip 1.2 (Bionano Genomics 20319). Single molecules were imaged and digitized using the Saphyr instrument. The output data were used for assembly into genome maps for structural variant detection with the Bionano Access software version 1.4.3.

Detection of Structural Variants by 10× Genomics

The 10× Chromium Genome Solution platform was utilized to detect structural variants and phase the variants in the patient's genome. The platform is an automated microfluidic system that allows for functionalized gel beads to be combined with high-molecular-weight DNA and oil to form a gel bead in emulsion (GEM). Isothermal incubation allows for the addition of a unique barcode to all DNA within the GEM.

Assessment of 10× Genomics Data

The whole-genome sequencing function of Long Ranger (v2.2.2) was used to analyze FASTQ data from 9p.101.p1. We used the supplied hg38 reference provided by 10× Genomics (<http://cf.10xgenomics.com/supp/genome/refdata-GRCh38-2.1.0.tar.gz>) and generated a phased BAM file and Loupe file. The breakpoint was identified in the Loupe genome browser (v2.1.1). We utilized Mosdepth (v0.2.3) (Pedersen and Quinlan 2018) to calculate read depth in 500-bp windows across the genome.

Calling Variants

Variant callers FreeBayes (v1.3.2-38-g71a3e1c) (Garrison and Marth 2012), Platypus (v1.0.2) (Rimmer et al. 2014), GATK (v 4.1.0.0) (McKenna et al. 2010), and Strelka2 (v2.9.2) (Kim et al. 2018) were run on the phased BAM file to generate SNVs and indels. The output vcf files were left-aligned, normalized, and then combined using GATK CombineVariants. SnpEff (v4.3T) (Cingolani et al. 2012) was used to annotate the combined variant files. We only considered variants that were identified in all four callers.

Literature Search of Affected Genes

We developed a custom search to compare patient phenotypes with genes affected by the deletion and duplication. First, genes within the deletion and duplication regions were searched using an automated PubMed abstract counting program (https://github.com/tycheletumer/pubmed_abstract_counter). This program counts the number of abstracts identified in PubMed for any given query. Our query was in the form of "gene AND phenotype" for each gene in the regions and for each phenotype in the individual. The phenotypes considered were dysmorphic facial features, increased nuchal skin folds, left posterior polydactyly, polydactyly, bicuspid aortic valve, coarctation of the aorta, development(al) delay, recurrent ear infections, ear infections, hearing loss, scoliosis, vertebral abnormalities, hemivertebrae, butterfly vertebrae, and superior mesenteric artery syndrome. Second, any query with at least one abstract in PubMed was then manually checked by a review of each abstract and paper. Those which survived manual review were shown in the table.

Loss-of-Function Variants in the Genome

We reduced our set of SNV and indels data sets by focusing on those that had the support of all four-variant callers to achieve maximal specificity. We then kept only the loss-of-function mutations (i.e., frameshift, stop-gained, splice-acceptor, splice-donor) and ran the gene list through eDGAR (http://edgar.biocomp.unibo.it/gene_disease_db/) (Babbi et al. 2017) to search for disease gene associations. Finally, we looked at the allele frequency of the variant in gnomAD version 3 (<https://gnomad.broadinstitute.org/>) (Karczewski et al. 2019) and removed variants with allele frequency of >1% in the database.

ADDITIONAL INFORMATION

Data Deposition and Access

Data are consented for sharing in a controlled-access database and are available at dbGaP (<https://www.ncbi.nlm.nih.gov/gap/>) under accession number SCV001251650.

Ethics Statement

This study was approved by the IRB (IRB ID #201102181 and ID #201706062) at the Washington University School of Medicine and written informed consent for this study was obtained from the patient's parents.

Acknowledgments

We thank our patient and family for participating in this study.

Author Contributions

F.S.C. and T.N.T. were involved in the design of the study and supervised the work. J.N., E.S., and T.N.T. were involved in the analysis of all data sets, and M.K., T.L., and R.F. contributed to the analysis of the Bionano data. D.B., D.J.W., and F.S.C. gathered patient and clinical information. J.N., E.S., and T.N.T. contributed to the writing of this work, and all authors were involved in the review of the manuscript.

Competing Interest Statement

The authors have declared no competing interest.

Received February 21, 2020;
accepted in revised form
April 27, 2020.

Funding

This study was supported by a National Institutes of Health (NIH) grant R00MH117165 to T.N.T. and a grant from the Children's Discovery Institute (F.S.C., D.J.W.).

REFERENCES

- Alfi O, Donnell GN, Crandall BF, Derencsenyi A, Menon R. 1973. Deletion of the short arm of Chromosome no.9 (46,9p-): a new deletion syndrome. *Ann Genet* **16**: 17–22.
- Alfi OS, Donnell GN, Allderdice PW, Derencsenyi A. 1976. The 9p- syndrome. *Ann Genet* **19**: 11–16.
- Babbi G, Martelli PL, Profiti G, Bovo S, Savojardo C, Casadio R. 2017. eD GAR: a database of Disease–Gene Associations with annotated Relationships among genes. *BMC Genomics* **18**: 554. doi:10.1186/s12864-017-3911-3
- Bi W, Borgan C, Pursley AN, Hixson P, Shaw CA, Bacino CA, Lalani SR, Patel A, Stankiewicz P, Lupski JR, et al. 2013. Comparison of chromosome analysis and chromosomal microarray analysis: what is the value of chromosome analysis in today's genomic array era? *Genet Med* **15**: 450–457. doi:10.1038/gim.2012.152
- Christ LA, Crowe CA, Micale MA, Conroy JM, Schwartz S. 1999. Chromosome breakage hotspots and delin-eation of the critical region for the 9p- deletion syndrome. *Am J Hum Genet* **65**: 1387–1395. doi:10.1086/302606
- Cingolani P, Platts A, Wang le L, Coon M, Nguyen T, Wang L, Land SJ, Lu X, Ruden DM. 2012. A program for annotating and predicting the effects of single nucleotide polymorphisms, SnpEff: sNPs in the genome of *Drosophila melanogaster* strain *w*¹¹¹⁸; *iso-2*; *iso-3*. *Fly (Austin)* **6**: 80–92. doi:10.4161/fly.19695
- Daiger SP, Sullivan LS, Bowne SJ, Cadena ED, Koboldt D, Bujakowska KM, Pierce EA. 2019. Detection of large structural variants causing inherited retinal diseases. *Adv Exp Med Biol* **1185**: 197–202. doi:10.1007/978-3-030-27378-1_32
- Demaerel W, Mostovoy Y, Yilmaz F, Vervoort L, Pastor S, Hestand MS, Swillen A, Vergaelen E, Geiger EA, Coughlin CR, et al. 2019. The 22q11 low copy repeats are characterized by unprecedented size and structural variability. *Genome Res* **29**: 1389–1401. doi:10.1101/gr.248682.119
- Eichler EE. 2019. Genetic variation, comparative genomics, and the diagnosis of disease. *N Engl J Med* **381**: 64–74. doi:10.1056/NEJMra1809315
- Garrison E, Marth G. 2012. Haplotype-based variant detection from short-read sequencing. arXiv 1207.3907.

- Hauge X, Raca G, Cooper S, May K, Spiro R, Adam M, Martin CL. 2008. Detailed characterization of, and clinical correlations in, 10 patients with distal deletions of Chromosome 9p. *Genet Med* **10**: 599–611. doi:10.1097/GIM.0b013e31817e2bde
- Huret JL, Leonard C, Forestier B, Rethore MO, Lejeune J. 1988. Eleven new cases of del(9p) and features from 80 cases. *J Med Genet* **25**: 741–749. doi:10.1136/jmg.25.11.741
- Karczewski KJ, Francioli LC, Tiao G, Cummings BB, Alföldi J, Wang Q, Collins RL, Laricchia KM, Ganna A, Birnbaum DP, et al. 2019. Variation across 141,456 human exomes and genomes reveals the spectrum of loss-of-function intolerance across human protein-coding genes. bioRxiv 531210. doi:10.1101/531210
- Kawara H, Yamamoto T, Harada N, Yoshiura K, Niikawa N, Nishimura A, Mizuguchi T, Matsumoto N. 2006. Narrowing candidate region for monosomy 9p syndrome to a 4.7-Mb segment at 9p22.2-p23. *Am J Med Genet A* **140**: 373–377. doi:10.1002/ajmg.a.31094
- Kim S, Scheffler K, Halpern AL, Bekritsky MA, Noh E, Kallberg M, Chen X, Kim Y, Beyter D, Krusche P, et al. 2018. Strelka2: fast and accurate calling of germline and somatic variants. *Nat Methods* **15**: 591–594. doi:10.1038/s41592-018-0051-x
- McKenna A, Hanna M, Banks E, Sivachenko A, Cibulskis K, Kernytsky A, Garimella K, Altshuler D, Gabriel S, Daly M, et al. 2010. The Genome Analysis Toolkit: a MapReduce framework for analyzing next-generation DNA sequencing data. *Genome Res* **20**: 1297–1303. doi:10.1101/gr.107524.110
- Mitsui N, Shimizu K, Nishimoto H, Mochizuki H, Iida M, Ohashi H. 2013. Patient with terminal 9 Mb deletion of Chromosome 9p: refining the critical region for 9p monosomy syndrome with trigonocephaly. *Congenit Anom (Kyoto)* **53**: 49–53. doi:10.1111/j.1741-4520.2012.00362.x
- Pedersen BS, Quinlan AR. 2018. Mosdepth: quick coverage calculation for genomes and exomes. *Bioinformatics* **34**: 867–868. doi:10.1093/bioinformatics/btx699
- Rimmer A, Phan H, Mathieson I, Iqbal Z, Twigg SR, Wilkie AO, McVean G, Lunter G. 2014. Integrating mapping-, assembly- and haplotype-based approaches for calling variants in clinical sequencing applications. *Nat Genet* **46**: 912–918. doi:10.1038/ng.3036
- Robinson JT, Thorvaldsdottir H, Winckler W, Guttman M, Lander ES, Getz G, Mesirov JP. 2011. Integrative genomics viewer. *Nat Biotechnol* **29**: 24–26. doi:10.1038/nbt.1754
- Swinkels ME, Simons A, Smeets DF, Vissers LE, Veltman JA, Pfundt R, de Vries BB, Faas BH, Schrandt-Stumpel CT, McCann E, et al. 2008. Clinical and cytogenetic characterization of 13 Dutch patients with deletion 9p syndrome: delineation of the critical region for a consensus phenotype. *Am J Med Genet A* **146a**: 1430–1438. doi:10.1002/ajmg.a.32310